Unique structural features of the AIPL1–FKBP domain that support prenyl lipid binding and underlie protein malfunction in blindness

Ravi P. Yadav[a], Lokesh Gakhar[b,c], Liping Yu[b,d], and Nikolai O. Artemyev[a,e,1]

[a]Department of Molecular Physiology and Biophysics, University of Iowa Carver College of Medicine, Iowa City, IA 52242; [b]Department of Biochemistry, University of Iowa Carver College of Medicine, Iowa City, IA 52242; [c]Protein Crystallography Facility, University of Iowa Carver College of Medicine, Iowa City, IA 52242; [d]NMR Core Facility, University of Iowa Carver College of Medicine, Iowa City, IA 52242; and [e]Department of Ophthalmology and Visual Sciences, University of Iowa Carver College of Medicine, Iowa City, IA 52242

Edited by Wolfgang Baehr, University of Utah, Salt Lake City, UT, and accepted by Editorial Board Member Jeremy Nathans July 3, 2017 (received for review March 23, 2017)

FKBP-domain proteins (FKBPs) are pivotal modulators of cellular signaling, protein folding, and gene transcription. Aryl hydrocarbon receptor-interacting protein-like 1 (AIPL1) is a distinctive member of the FKBP superfamily in terms of its biochemical properties, and it plays an important biological role as a chaperone of phosphodiesterase 6 (PDE6), an effector enzyme of the visual transduction cascade. Malfunction of mutant AIPL1 proteins triggers a severe form of Leber congenital amaurosis and leads to blindness. The mechanism underlying the chaperone activity of AIPL1 is largely unknown, but involves the binding of isoprenyl groups on PDE6 to the FKBP domain of AIPL1. We solved the crystal structures of the AIPL1–FKBP domain and its pathogenic mutant V71F, both in the apo form and in complex with isoprenyl moieties. These structures reveal a module for lipid binding that is unparalleled within the FKBP superfamily. The prenyl binding is enabled by a unique "loop-out" conformation of the β4-α1 loop and a conformational "flip-out" switch of the key W72 residue. A second major conformation of apo AIPL1–FKBP was identified by NMR studies. This conformation, wherein W72 flips into the ligand-binding pocket and renders the protein incapable of prenyl binding, is supported by molecular dynamics simulations and appears to underlie the pathogenicity of the V71F mutant. Our findings offer critical insights into the mechanisms that underlie AIPL1 function in health and disease, and highlight the structural and functional diversity of the FKBPs.

FKBP | photoreceptor | chaperone | PDE6 | AIPL1

FKBP-domain–containing proteins (FKBPs), whose prototypic member is FKBP12, play pivotal roles in cellular signaling, protein folding, and transcription (1–4). In addition to playing these intrinsic cellular roles, FKBPs mediate the effects of the immunosuppressive drugs FK506 and rapamycin (5, 6). Binding of FK506 to FKBP12 creates an interface for calcineurin, whereas binding of rapamycin enables interaction with and inhibition of mammalian target of rapamycin; thus, FKBP12 can initiate two distinct immunosuppressive pathways (7). Many FKBPs are peptidylprolylisomerases (PPIases) that catalyze the *cis–trans* conversion of peptidylprolyl bonds (8). A wealth of structural information on FKBPs and their complexes with drugs has been gathered over the years. A classic FKBP domain fold is comprised of a half-conical six-stranded β-sheet surrounding a short central α-helix. Both FK506 and rapamycin bind within a prominent and highly conserved hydrophobic cavity between the β-sheet and the α-helix (5). These drugs also contact a hairpin loop of ∼20 aa that links β-strands β5 and β6 and hangs over the cavity (Fig. 1*C*). Surprisingly, other than the fact that this pocket contributes to the PPIase active site (9), very little is known about its physiological significance or its natural ligands. One of the few examples of such ligands is the type I TGFβ receptor, to which FKBP12 binds via its hydrophobic pocket and hairpin loop (10).

Notably, one member of the FKBP family is known to play a unique biological role and has a known native ligand, yet virtually no structural information is available to shed light on the mechanisms underlying its function. This protein, aryl hydrocarbon receptor-interacting protein-like 1 (AIPL1), was discovered because of the association of mutations in the encoding gene with one of the most severe forms of Leber congenital amaurosis (LCA), an early-onset inherited retinopathy and one of the main causes of blindness in children (11–15). AIPL1 shares domain organization (an FKBP domain and a tetratricopeptide repeat domain) and 50% sequence identity with aryl hydrocarbon receptor-interacting protein (AIP) (11). However, AIPL1 (11, 16) is retina-specific, whereas AIP is expressed in various tissues, where it acts as a cochaperone with HSP90 in the maturation of aryl hydrocarbon receptor and other nuclear receptors (17). The FKBP domains of AIPL1 and AIP are unusual in several respects, most importantly that they neither bind FK506 nor have PPIase activity, and they have long "insert" regions of equivalent lengths (57 aa) that replace the hairpin loop of classic FKBPs (Fig. 1*D*) (18, 19). The mechanism whereby AIPL1 exerts its biological effects remained obscure until an AIPL1 knockout mouse model revealed that the rapid retinal degeneration that characterizes this disease is caused by marked reduction in protein levels and activity of the phototransduction effector enzyme phosphodiesterase 6 (PDE6) (20, 21). The resulting hypothesis that AIPL1 is a chaperone for PDE6 was recently validated by the demonstration that AIPL1 is required for heterologous expression of functional PDE6 (22). This chaperone activity involves interaction of the FKBP domain with the farnesyl, and geranylgeranyl modifications of the catalytic subunits of PDE6 (23, 24). Interestingly, AIP fails to appreciably bind the isoprenyl moieties and to chaperone PDE6 (22), indicating that the AIPL1–FKBP domain is uniquely specialized.

Significance

Mutations in the gene encoding aryl hydrocarbon receptor-interacting protein-like 1 (AIPL1) disrupt the ability of this protein to function as a chaperone of prenylated photoreceptor phosphodiesterase 6, and cause a severe form of childhood blindness. Our discovery of two features—the unique structure of the AIPL1–FKBP domain essential for its binding of prenyl lipids, and the unusual conformational dynamics altered by pathogenic mutations—advances our understanding of both the protein structure and dynamics required for prenyl binding. Moreover, our studies provide a molecular mechanism underlying the blindness disease.

Author contributions: R.P.Y., L.G., L.Y., and N.O.A. designed research, performed research, analyzed data, and wrote the paper.

The authors declare no conflict of interest.

This article is a PNAS Direct Submission. W.B. is a guest editor invited by the Editorial Board.

Data deposition: The atomic coordinates have been deposited in the Protein Data Bank, www.pdb.org (PDB ID codes 5U9A, 5U9I, 5U9J, 5U9K, and 5V35).

[1]To whom correspondence should be addressed. Email: nikolai-artemyev@uiowa.edu.

This article contains supporting information online at www.pnas.org/lookup/suppl/doi:10.1073/pnas.1704782114/-/DCSupplemental.

www.pnas.org/cgi/doi/10.1073/pnas.1704782114

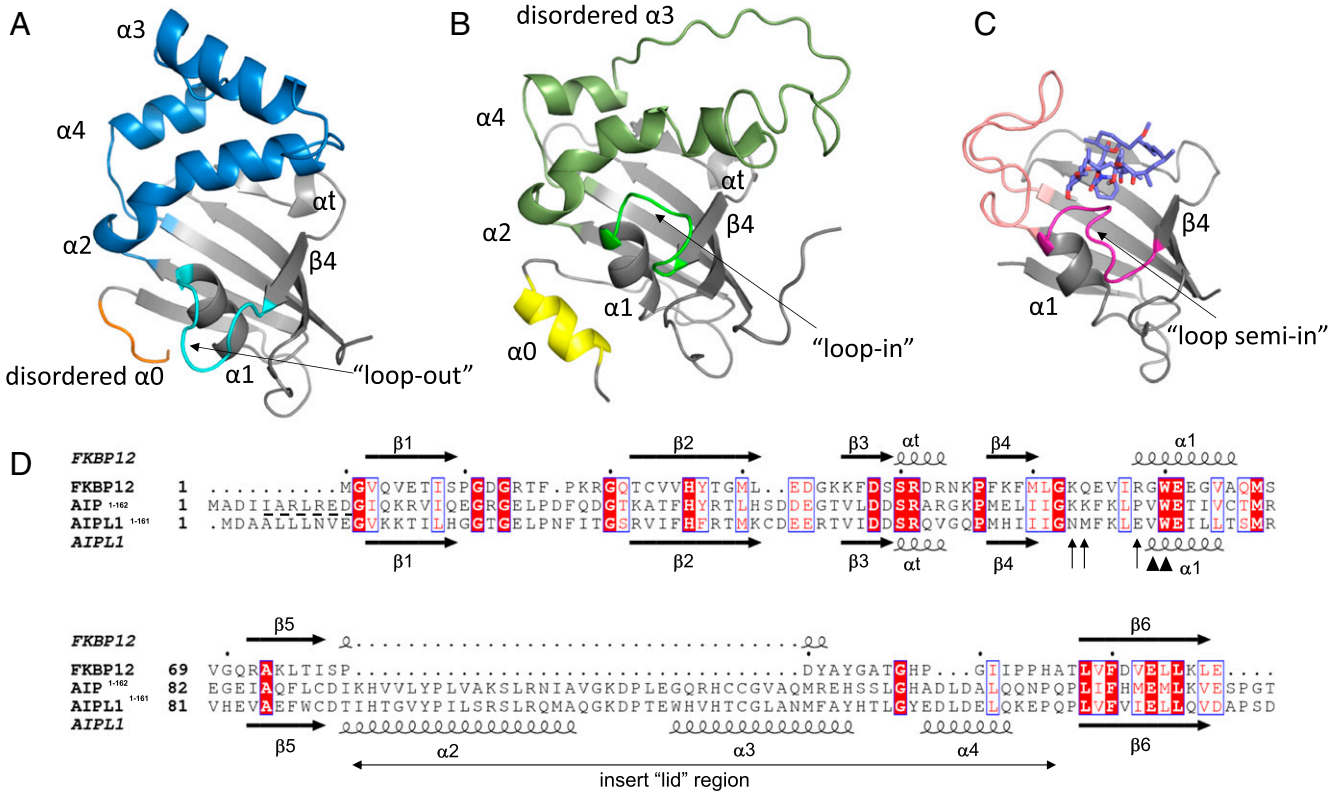

Fig. 1. Comparison of FKBP-domain structures of AIPL1, AIP, and FKBP12. (*A*) AIPL1 (PDB ID code 5U9A). Highlighted are the 57-residue insert region (blue), which forms three α helices α2, α3, and α4); the β4-α1 loop (cyan), which is in the loop-out conformation; and the N-terminal α0 region (orange), which is disordered. (*B*) AIP (PDB ID code 2LKN). Highlighted are the 57-residue insert region (faded green), whose α3 helix region is disordered; the β4-α1 loop (bright green), which is in a loop-in conformation; and the α0 region (yellow), which is structured. (*C*) FKBP12 (PDB ID code 1FKB). Highlighted are the 20-residue hairpin loop counterpart to the insert region in AIPL1 and AIP (salmon); the β4-α1 loop (magenta), which is in a loop semi-in conformation; and rapamycin (indicated in purple stick representation). (*D*) Sequence alignment of human FKBP12 with the FKBP-domains of AIP and AIPL1. The key elements of the protein secondary structure are identified. A single-turn α-helix between the β3 and β4 strands is denoted as αt. Arrowheads indicate AIPL1 residues V71 (mutated in LCA) and W72 (flips between two conformations, as detected by NMR). Arrows indicate residues in the β4-α1 loop that differ between AIPL1 and AIP, and contribute to the loop-out or loop-in conformation. Dashed underline highlights the α0-helix region, which is α-helical in AIP but not in AIPL1. The well-ordered α3 helix in AIPL1 corresponds to the poorly ordered flexible region in AIP.

To gain mechanistic insights into the function of AIPL1 and its key interaction with isoprenylated PDE6, we solved the crystal structures of AIPL1–FKBP in the apo form and in complex with S-farnesyl-L-cysteine methyl ester (FC) and geranylgeranyl pyrophoshate (GGpp), along with the crystal structures of apo and FC-liganded V71F mutant, which is linked to LCA. These structures exposed remarkable features of AIPL1–FKBP that enable isoprenoid moieties to bind to a deep hydrophobic pocket formed by the core FKBP fold and the insert region. The molecular determinants of the unique ligand-binding properties of AIPL1 that were suggested by the structures were validated by a loss-of-function mutational analysis. Furthermore, we present NMR analyses of the AIPL1–FKBP and V71F proteins in solution. Our data reveal that the AIPL1–FKBP protein is present in two major conformations in solution, and that in the LCA-associated mutant the W72 side chain is predominantly oriented into the ligand-binding pocket, thus capable of blocking ligand binding. These conclusions regarding the mechanism that leads to LCA are reinforced by results from molecular dynamics (MD) simulations. Collectively, our studies provide critical insights into AIPL1 function in health and disease, and highlight the structural and functional diversity of the FKBP proteins.

Results

Structure of Apo AIPL1–FKBP and Its Unique Features. The crystal structure of AIPL1–FKBP was solved at 2.70 Å, to an *R*-factor of 21.2% and *R*-free of 28.9% (Table 1). The protein crystallized in a $C222_1$ space group, with a single molecule in the asymmetric unit. The diffraction pattern was strongly anisotropic, but it was possible to determine the structure using molecular replacement. Residues 6–160 could be modeled clearly based on the electron density. The structure of AIPL1–FKBP that was gleaned from this analysis was the classic FKBP fold, with six antiparallel β-strands enclosing a central α-helix (α1), and an insert region (albeit distinct from that observed in AIP) that covers the conical half β-barrel and the hydrophobic cavity (Fig. 1*A*).

Overall, this crystal structure resembles the NMR-derived structure of AIP (2LKN) (18), with the exception of three segments: the N terminus, the β4-α1 loop (residues 64–70) that precedes α1, and the "insert" region (residues 90–146) (Fig. 1 *A* and *B*). Two of the three regions of interest, the N terminus and the β4-α1 loop, are unaffected by lattice contacts and free to sample conformations other than those observed in the crystal structure. The α3 helix from the insert region interacts with α3 of a neighboring molecule (*SI Appendix*, Fig. S1). In the case of the N terminus, in AIP these residues form an α-helix (α0) that runs antiparallel to the first β-strand and α1, and apparently stabilizes the protein (Fig. 1*B*) (18); in AIPL1 the corresponding sequence produces no regular secondary structure, although its orientation is similar to that of AIP α0 (Fig. 1*A*). In the case of the insert region, that of AIP begins and ends with an α-helix, but the middle portion is unstructured and highly-flexible (Fig. 1*B*). In contrast, in AIPL1 the insert region is well-structured and comprised of three α-helices: α2, α3, and α4 (Fig. 1*A*). Furthermore, in AIPL1 the α-helices at the start and end of the insert region are tilted away from the center of the hydrophobic cavity relative to their positions in AIP. The most striking, and

Table 1. Crystallographic data collection and refinement statistics of FKBP domain of AIPL1

Data collection, refinement, and Ramachandran plot	AIPL1-FKBP	AIPL1-FKBP:FC	AIPL1-FKBP:GGpp	AIPL1-FKBP V71F	AIPL1-FKBP V71F:FC
PDB ID code	5U9A	5U9I	5U9J	5U9K	5V35
Data collection statistics					
Wavelength	1.00	1.00	1.00	1.00	1.00
Space group	$C222_1$	$C222_1$	$C121$	$C222_1$	$C222_1$
Cell dimensions (Å, °)	a = 52.10	a = 54.97	a = 69.34	a = 51.79	a = 53.15
	b = 65.74	b = 66.18	b = 51.17	b = 65.07	b = 65.52
	c = 107.04	c = 106.96	c = 106.97	c = 106.18	c = 106.95
			β = 93.09		
Resolution (Å)	53.52–2.70 (2.85–2.70)	42.29–2.30 (2.42–2.30)	41.15–2.10 (2.21–2.10)	40.52–2.70 (2.85–2.70)	53.47–2.50 (2.60–2.50)
R_{merge}	0.077 (0.692)	0.115 (1.06)	0.078 (0.692)	0.064 (0.787)	0.059 (0.069)
$I/\sigma(I)$	24.9 (4.4)	15.60 (3.20)	17.5 (3.00)	23.30 (3.20)	23.60 (2.80)
Completeness (%)	100.0 (99.9)	99.90 (99.90)	97.70 (97.70)	99.90 (99.70)	99.80(99.90)
Redundancy	13.8 (13.0)	13.30 (13.10)	6.90 (6.70)	12.40 (11.60)	13.80(13.00)
Refinement statistics					
Resolution (Å)	53.52–2.70	42.29–2.30	41.15–2.10	40.52–2.70	53.47–2.50
Number of reflections	5,026	8,925	21,346	4,926	6,393
R_{work}/R_{free} (%)	21.20/28.90	23.50/26.60	23.80/29.40	20.10/ 25.70	21.60/27.20
B-factor (Å^2)					
Protein	77.63	57.92	34.15 (A)	84.84	80.88
			33.06 (B)		
Ligand	—	67.70	41.87 (A)	—	96.87
			48.42 (B)		
Water	—	—	36.04 (A)	—	—
			35.76 (B)		
Rmsd					
Bond length (Å)	0.010	0.011	0.014	0.012	0.014
Bond angles (°)	1.463	1.191	1.29	1.598	1.729
No. of atoms					
Protein	1,230	1,205	1,195 (A)	1,246	1,174
			1,207 (B)		
Ligand	0	15	20 (A)	0	15
			20 (B)		
Water	0	0	66 (A)	0	0
			75 (B)		
Metal	0	0	1	0	0
Ramachandran plot (% residues)					
Most favored	89.89	91.89	93.67	91.5	91.33
Allowed	9.80	8.11	6.33	5.89	8.00
Disallowed	1.31	0	0	2.61	0.67

apparently critical, difference is in the β4-α1 loop (Figs. 1 *A* and *B* and 2). In AIP, this loop is in the "loop-in" conformation, where it interacts with α2 of the insert region (Fig. 1*B*). In particular, the loop residues F68 and L70 make hydrophobic contacts with L97, Y98, V101, and L105 from α2, whereas K69 appears to form a hydrogen bond with S104. These interactions allow the insert region and the loop to seal the hydrophobic cavity and make it inaccessible from the surface (Fig. 2*A*). In comparison, the β4-α1 loop in AIPL1 does not obstruct the cavity entrance, and adopts a markedly different "loop-out" conformation (Fig. 1*A*), characterized by two distinct narrow openings into the hydrophobic cavity (Fig. 2*B*). In this protein, the cavity is formed by: the hydrophobic residues F35, F37, M59, I61, F87 C89, F149, and I151 in the half β-barrel; residues V71, W72, L75, and L76 of α1; and V96, Y97, L100, L104, M107 of α2 (insert region). In the loop-out conformation, α1 is tilted slightly away from the half β-barrel, and the essential residue W72 undergoes a hinge-like rotation (Fig. 2*C*). The side chains of the corresponding residues in AIP (W73) and FKPB12 (W59) are perpendicular to the axis of α1 ("flipped into" the cavity), and form the base of the cavity (Fig. 2*C*). The rotation of W72 in AIPL1 to a position parallel to the axis of α1 ("flipping out" of the cavity), together with the movement of α1, deepen the pocket (Fig. 2*C*).

Structures of FC- and GGpp-Bound AIPL1–FKBP: Molecular Determinants of Ligand Selectivity. The AIPL1–FKBP:FC crystal structure was also solved in the $C222_1$ space group, to a resolution of 2.30 Å. Because the dimensions of the cells in the FC crystal were similar to those in the apo crystal, rigid body refinement of the apo structure was sufficient for locating the single molecule in the asymmetric unit. Restrained refinement using Refmac and phenix.refine, followed by fitting in Coot, resulted in a final *R*-factor of 23.5% and an *R*-free of 26.6% (Table 1). Besides the presence of the ligand, there are no significant differences between the apo and FC-bound structures (*SI Appendix*, Fig. S2). In the final refined structure, the ligand density in the vicinity of W72 was sufficient to allow modeling of the farnesyl portion of FC with confidence (*SI Appendix*, Fig. S3 *A* and *B*). In addition to FC contacts within the ligand-binding site (*SI Appendix*, Fig. S4), the Cys end of FC makes lattice contacts with the α2-α3 turn of a neighboring molecule, which are not likely to influence the binding of the farnesyl region (*SI Appendix*, Figs. S5 and S6).

The AIPL1–FKBP:GGpp crystal was solved in the *C2* space group to a resolution of 2.10 Å, with two molecules in the

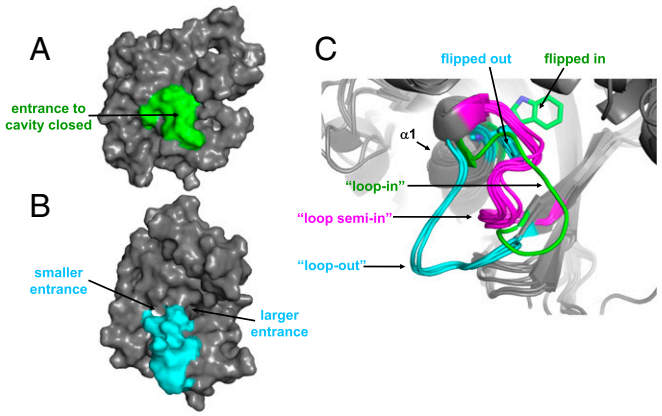

Fig. 2. Hydrophobic cavity access and the role of the β4-α1 loop and the α1 tryptophan residue. (*A* and *B*) The FKBP domains of AIP and AIPL1 shown in surface representation. In AIP, the hydrophobic cavity is sealed from the surface because of the loop-in conformation of β4-α1 (*A*), but in AIPL1 the loop-out conformation of β4-α1 provides two entrances to the cavity (*B*). (*C*) Comparison of the β4-α1 loop, showing that irrespective of the presence or absence of ligands, in most FKBP proteins it is in the loop semi-in conformation (magenta; PDB ID codes 1C9H, 1FKB, 1Q1C, 2PBC, 2PPN, 2VN1, 3JYM), in AIP it is in the loop-in conformation (green; PDB ID code 2LKN), and in AIPL1 it is in the loop-out conformation (cyan; PDB ID codes 5U9A, 5U9I, 5U9J). In AIP, the side chain of W73 (green sticks) is flipped into the cavity and forms its base, whereas in AIPL1 W72 (cyan sticks) is flipped out and thus the cavity is deeper.

asymmetric unit, and it was refined to a *R*-factor of 23.8% and an *R*-free of 29.4% (Table 1). Other than a packing-induced shift of α3 and minor conformational changes in the ligand binding site, the structures of AIPL1–FKBP bound to GGpp and FC did not differ significantly (*SI Appendix*, Fig. S2). The geranylgeranyl portion of GGpp was reliably modeled into the ligand density in the final refined structure (*SI Appendix*, Fig. S3 *C* and *D*). As also seen for FC, the prenyl group of GGpp is involved in van der Waals interactions with W72 at the entrance of the hydrophobic pocket. The longer GG moiety appears to extend deeper into the binding cavity than FC (Fig. 3 *A* and *B* and *SI Appendix*, Fig. S4). The binding of FC or GGpp to AIPL1–FKBP did not appear to change the volume of the ligand binding pocket as determined by calculating solvent probe-accessible volume with VOIDOO (*SI Appendix*, Fig. S7) (25).

Our comparison of the structures of AIPL1–FKBP and AIP–FKBP suggests that the capacity for isoprenyl ligand binding is determined by distinct conformations of the β4-α1 loop in the core domain, by the insert region, or by both. To probe the determinants of ligand selectivity, we constructed two chimeric full-length proteins: chimeric AIP (chi-AIP), which contains the insert region of AIPL1; and its reciprocal chimera, chi-AIPL1, which contains the insert region of AIP. The binding of FC to AIPL1, AIP, chi-AIP, and chi-AIPL1 was measured using a fluorescence polarization assay using the FITC-labeled FC-probe (FC-FITC). This analysis revealed AIPL1 to bind FC-FITC with a K_d of 125 ± 5 nM, and AIP to bind the probe very poorly (K_d > 3 μM) (*SI Appendix*, Fig. S8). Both chi-AIP and chi-AIPL1 bound FC-FITC more effectively than did AIP, although chi-AIPL1 bound the probe more weakly than did AIPL1 (K_d 815 ± 20 nM) but more strongly than did chi-AIP (K_d 1,475 ± 215 nM) (*SI Appendix*, Fig. S8). These results suggest that both the core domain and insert region of FKBP contribute to ligand selectivity, with the core domain playing a greater role. The sequence of the AIPL1 β4-α1 loop differs from that in AIP at three positions: N65(K66), M66(K67), and E70(P71) (Fig. 1*D* and *SI Appendix*, Fig. S9). In particular, P71 may prevent the loop in AIP from assuming a loop-out conformation. We next examined if the AIPL1→AIP conversion of the β4-α1 loop affects binding to FC-FITC. Analysis of the AIPL1–FKBP triple mutant N65K/M66K/E70P revealed marked attenuation of the affinity for the probe (K_d 795 ± 65 nM vs. 50 ± 6 nM), confirming that the β4-α1 loop plays a crucial role in ligand binding (Fig. 3*C*).

Given the strong decrease in the ligand interaction that was observed in the case of the AIPL1–FKBP N65K/M66K/E70P mutant, we tested the ability of the triple mutant of the full-length AIPL1 to chaperone PDE6. To this end, we used cultured HEK293T cells transfected with PDE6C and Pγ in the absence and presence of the WT and N65K/M66K/E70P forms of AIPL1 (22). In lysates of HEK293T cells cotransfected with PDE6C and Pγ, cGMP hydrolysis did not exceed the very low levels in lysates from untransfected cells (7.6 ± 2.7 pmol cGMP hydrolyzed per milligram protein per minute). Consistent with previous observations (22), coexpression of PDE6C and Pγ with WT AIPL1 led to robust cGMP hydrolysis in cell lysates (14.7 ± 1.2 nmol cGMP hydrolyzed per milligram protein per minute). In cells coexpressing PDE6C, Pγ, and the N65K/M66K/E70P mutant, cGMP hydrolysis was about 90-fold lower (0.16 ± 0.03 nmol cGMP hydrolyzed per milligram protein per minute). Immunofluorescence and Western blot analyses indicated that subcellular distribution and the protein expression level of N65K/M66K/E70P

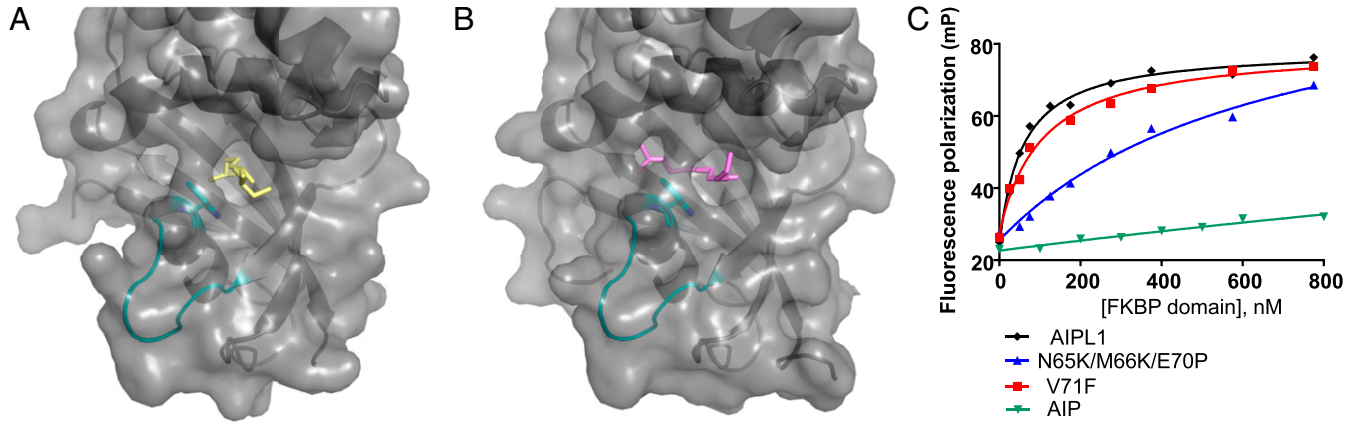

Fig. 3. FC- and GGpp-bound structures of AIPL1. (*A* and *B*) The farnesyl moiety of FC (yellow) (*A*), and the geranylgeranyl moiety of GGpp (pink) (*B*) penetrate the hydrophobic binding pocket, with the latter sitting deeper. In both cases, W72 (cyan) is flipped out, and thus the ligands can enter the cavity. (*C*) Binding of FC-FITC to the AIP–FKBP domain, the AIPL1–FKBP domain, and two mutant forms of the latter (N65K/M66K/E70P and V71F). Fluorescence polarization (mP) of FC-FITC is plotted as a function of concentration of the binding protein, and data are fit using a single-site binding equation. The results of a representative experiment are shown. The K_d values, calculated based on three experiments, are: 50 ± 6 nM for AIPL1–FKBP; 795 ± 65 nM for AIPL1–FKBP N65K/M66K/E70P; 101 ± 13 nM for AIPL1–FKBP V71F, *t* test vs. AIPL1–FKBP significance value $P = 0.02$; and >5,000 nM for AIP–FKBP.

in transfected HEK293T cells were similar to those of the wild-type AIPL1 (*SI Appendix*, Fig. S10). Thus, the loss of ligand binding in this mutant AIPL1 dramatically impaired its ability to chaperone PDE6C.

The LCA-Linked W72S Mutant of AIPL1 Is Unstable at Physiological Temperature. Recently, we confirmed that three AIPL1 mutations linked to LCA (V71F, W72S, and C89R) are pathogenic, by demonstrating that they fail to chaperone PDE6 in HEK293T cells (22). W72S and C89R formed perinuclear aggregates, an outcome consistent with protein instability. However, the subcellular distribution of V71F was similar to that of the WT protein (22). Because the C89 side chain is buried in the hydrophobic cavity of the AIPL1–FKBP structure and the C89R mutant fails to bind FC (23), these data suggest that this mutation destabilizes the entire ligand-binding pocket. In contrast, V71F and W72S retained the capacity for prenyl-ligand binding at 25 °C (23). We therefore examined thermal stabilities of AIPL1–FKBP and its V71F and W72S mutants in the absence and presence of FC by measuring protein hydrodynamic radius with dynamic light scattering (DLS) while ramping the temperature. The thermal stabilities of AIPL1–FKBP (T_{onset} 45.6 °C) and V71F (T_{onset} 46.7 °C) were similar, and the proteins, particularly AIPL1–FKBP WT, were modestly stabilized by bound FC (*SI Appendix*, Fig. S11). Interestingly, W72S with the T_{onset} of 34 °C was clearly unstable at human body temperature, but the binding of FC increased the mutant stability by about 8 °C (*SI Appendix*, Fig. S11).

Structures of the AIPL1 V71F Mutant Linked to LCA. To gain insight into the mechanism whereby the V71F mutation leads to disease, we solved crystal structure of V71F in the apo form (PDB ID code 5U9K) and in complex with FC (PDB ID code 5V35) (Table 1). Surprisingly, no dramatic differences between these structures and the corresponding structures of AIPL1–FKBP were observed (*SI Appendix*, Fig. S2). The structure of V71F:FC was similar to that of AIPL1–FKBP:FC and it had a clear electron density for the ligand to be modeled (*SI Appendix*, Figs. S3 *E* and *F* and S4). The volume of the ligand-binding pocket in V71F appeared somewhat larger than that in AIPL1–FKBP WT (*SI Appendix*, Fig. S7). Thus, the crystal structures of V71F have not clearly revealed the underlying mechanism of this mutation. Our parallel efforts to obtain crystals of the W72S mutant of AIPL1–FKBP have not been successful.

Apo AIPL1–FKBP Has Two Major Conformations in Solution. NMR studies were conducted to investigate the structure of AIPL1–FKBP in solution and the effects of the V71F mutation. We had previously made backbone and side-chain assignments for a human AIPL1–FKBP construct (residues 2–161) in which residues 111–132 were deleted and replaced with a short loop consisting of five glycines (AIPL1–FKBP$^{\Delta 111-132}$) (26). Overlay of the $^{15}N/^{1}H$ HSQC spectra of AIPL1–FKBP and AIPL1–FKBP$^{\Delta 111-132}$ in complex with FC revealed that the spectra are nearly identical, except for about a dozen shifted peaks and a dozen extra peaks present in the AIPL1–FKBP protein as a result of the presence of residues 111–132 (26). Thus, the majority of the assigned peaks in the spectra of the AIPL1–FKBP$^{\Delta 111-132}$:FC complex can be straightforwardly transferred to the corresponding residues in the AIPL1–FKBP:FC complex (Fig. 4). The mutation of selected residues, including I49L, I61L, L69A, and L104I in the AIPL1–FKBP domain confirmed the assignments of the methyl groups of these residues in the WT protein (*SI Appendix*, Figs. S12 and S13).

Overlay of $^{15}N/^{1}H$ HSQC spectra of AIPL1–FKBP in the absence and presence of FC indicates that there are two detected peaks for each backbone amide in the apo protein for the majority of the peaks. These dual peaks correspond to two protein conformations: an "open" conformation that may be similar to that observed in the crystal structure of apo AIPL1–FKBP; and a "closed" or "flip-in" conformation, in which the W72 side chain is rotated into the ligand-binding pocket (see below), thus mimicking the ligand. As a result, the positions of the peaks in the closed conformation nearly matched those in the FC-bound form (Fig. 4*A*, *Right*). Based on the intensities of the well-resolved peaks in the $^{15}N/^{1}H$ HSQC spectra, AIPL1–FKBP contains ∼30% open and 70% closed conformations. The notion that apo AIPL1–FKBP exists in two conformations is also supported by analysis of the side-chain methyl groups (Fig. 4 *B* and *C*). Importantly, upon FC-binding, the two conformations present in the apo AIPL1–FKBP protein converge into a single liganded conformation (Fig. 4).

The residues located in the ligand-binding pocket of apo AIPL1–FKBP exhibit extremely broad peaks. To trace the peak positions of these important residues in the apo protein, we performed ligand titration experiments using the soluble ligand geraniol, which has a much weaker binding affinity for AIPL1–FKBP (K_d = 1.2 mM as determined by NMR) than FC (Fig. 5 *A* and *B*). Two unliganded conformations in the apo protein were clearly detected for L100 $C_{\delta 2}H_3$, and these peaks are distinct from those in the ligand-bound conformation and were nearly broad beyond detection in the apo protein (Fig. 5 *A* and *B*). As the geraniol concentration increased during the titration, these two broad peaks gradually sharpened and moved toward that of the ligand-bound conformation (Fig. 5 *A* and *B*). These observations were validated by making the L100I mutant; in this mutant protein the $C_{\delta}H_3$ methyl peaks of L100 were absent (Fig. 5*C*).

The conformational heterogeneity of the AIPL1–FKBP apo protein is most likely a consequence of reorientation of the aromatic side chain of W72, which is juxtaposed below L100 (Fig. 5*D*), and whose flip-out and flip-in conformations could have resulted in the two detected conformations of the apo protein. The flip-out conformation of W72 is likely to be similar to the conformation of W72 detected in the crystal structures. The W72 flip-in conformation is not captured in the crystal structures. Although the closed (or flip-in) conformation of apo AIPL1–FKBP mimics the ligand-bound state in NMR spectra, these two conformations of closed vs. ligand-bound are principally different in that the W72 side chain is flipped-out when ligand is bound. The intermediate reorientation rate of W72 is likely the cause of the excessive line broadening of L100 methyl groups in the apo protein. This explanation is also consistent with the observation that indole ring NεH of W72 is broad beyond detection in the apo protein, as well as in complexes with FC or geraniol. In contrast, indole ring NεH peaks of W88 and W116 are clearly observed (26). Because the W72 is located at the central hydrophobic core formed between the core domain and cap domain of AIPL1–FKBP, its conformational heterogeneity has caused widespread peak splitting throughout the molecule.

The V71F Mutant Assumes the Closed Conformation in Solution. In contrast to the peak splitting/multiplicity and heterogeneity observed for the apo AIPL1–FKBP, the V71F mutant nearly quenched the peak splitting, thus exhibiting much better spectral quality in the apo form (*SI Appendix*, Fig. S14). The V71F mutation has caused convergence of the two detected conformations in the apo AIPL1–FKBP WT protein into mostly a single detected conformation. Like the WT form of AIPL1–FKBP, the V71F mutant binds to FC and the chemical shift perturbations induced by this binding can be traced for the well-resolved residues (*SI Appendix*, Fig. S15). Clearly, one of the largest perturbed residues upon FC binding is L100; this is consistent with the structure for AIPL1–FKBP:FC complex where L100 is found to interact with the bound prenyl moiety.

To determine the structural conformation of the V71F mutant in solution in the apo state, we studied side-chain methyl groups, using a ^{13}C-methyl–labeled sample for the IVL residues. The V71F mutant exhibited an upfield shift of the CH_3 groups of L75 relative to WT protein, because of the ring current effect of the substituted Phe. This finding is consistent with the helical structure of α1 (*SI Appendix*, Fig. S16 *A* and *B*). Interestingly, the V71F mutant also exhibited an upfield shift of the $C_{\delta}H_3$ group of I61, which is located on the opposite side of the V71F substitution (Fig. 6 *A* and *D*). However, upon FC binding, this upfield-shifted I61 $C_{\delta}H_3$ moved downfield (Fig. 6*C*), to a position that overlaps exactly with that of WT I61 $C_{\delta}H_3$ (Fig. 6*B*).

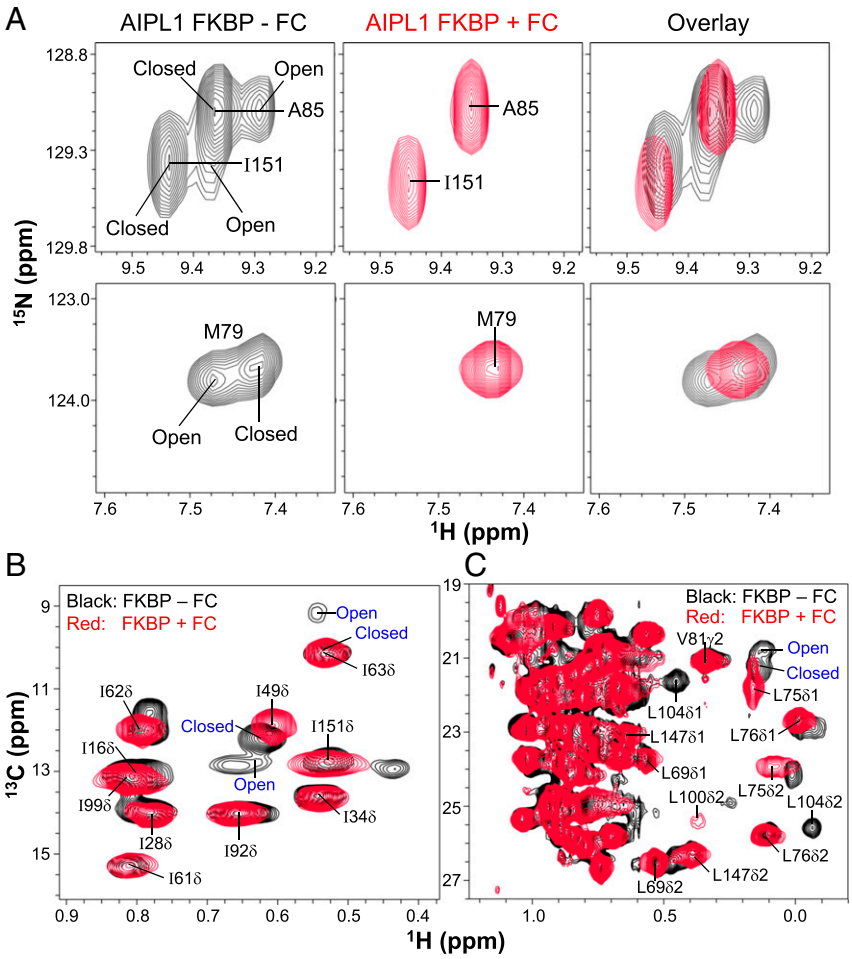

Fig. 4. Apo AIPL1–FKBP exists in two conformations in solution that collapse to one conformation on FC binding. (*A*) The M79, A85, and I151 amide regions of the ^{15}N/^{1}H HSQC spectra of AIPL1–FKBP in the absence and presence of FC and their spectra overlays. (*B* and *C*) Overlay of ^{13}C/^{1}H HSQC spectra of AIPL1–FKBP in the absence and presence of FC. (*B*) Ile $C_\delta H_3$ region. (*C*) Val $C_\gamma H_3$ and Leu $C_\delta H_3$ region. A subset of assigned peaks is labeled.

These data strongly indicate that in the apo V71F protein in solution the W72 side chain has rotated back into the ligand-binding pocket and thus has a flip-in major conformation (Fig. 6*D*). Therefore, the crystal structure of AIPL1–FKBP V71F appears to capture a minor state of the apo protein in solution, in which the W72 is flipped out (open conformation), whereas the NMR data detects a major state in which the side chain of W72 is flipped in (closed conformation). The fact that I74 $C_\delta H_3$ and L75 $C_\delta H_3$ of V71F are strongly shifted downfield upon FC binding (Fig. 6*C* and *SI Appendix*, Fig. S16*C*) suggests that the V71F Phe side chain moves further away from these two residues once FC is bound. The flip-in conformation of apo V71F is predicted to reduce FC binding, and we indeed detected a statistically significant, albeit a modest (~twofold) reduction in affinity of V71F for both FC-FITC (Fig. 3*C*) and FC-AMCA [6-((7-amino-4-methylcoumarin-3-acetyl)amino) hexanoic acid succinimidyl ester] (*SI Appendix*, Fig. S17).

The Triple Mutant N65K/M66K/E70P Has a W72 Flip-in and β4-α1 Loop-in Conformation in Solution. In the absence of FC, the triple mutant exhibits well-behaved and homogeneous peaks in the ^{15}N/^{1}H HSQC spectrum, contrasting to the peak splitting/multiplicity and conformational heterogeneity observed in the WT apo protein (*SI Appendix*, Fig. S18), indicating that the triple mutant has quenched conformational heterogeneity present in the apo WT protein. The triple mutant still binds to FC (*SI Appendix*, Fig. S19), but did not cause widespread chemical-shift perturbations in the ^{15}N/^{1}H HSQC spectrum as observed for the WT protein or V71F mutant, suggesting that FC did not penetrate deeply into the hydrophobic core of the triple mutant. Therefore, FC-binding to the triple mutant is expected to be shallow and weak in agreement with our fluorescence assay data (Fig. 3*C*). Using a ^{13}C-methyl-labeled triple mutant sample for the IVL residues, we found that I151 $C_\delta H_3$ is strongly upfield shifted by >0.6 ppm in ^{1}H in the triple mutant relative to the WT protein (*SI Appendix*, Fig. S20*A*), suggesting that the W72 aromatic ring has a flip-in conformation that sits directly over I151 as observed in the AIP–FKBP structure, such that the W72 aromatic ring induces a strong ring current for I151 $C_\delta H_3$. Moreover, the I61 $C_\delta H_3$ is also strongly shifted upfield by >0.5 ppm in ^{1}H in the apo state of triple mutant relative to the WT protein (*SI Appendix*, Fig. S20*A*), indicating that the β4-α1 loop consisting of K65-K66-F67-K68-L69-P70 (that mimics the loop in AIP–FKBP) in the triple mutant has a loop-in conformation and its F67 is juxtaposed above I61, as observed in the AIP–FKBP structure, such that F67 aromatic ring induces such a large ring current for I61 $C_\delta H_3$. These conformations result in a shallow and weak binding of FC. FC-binding also causes peak broadening of I61 $C_\delta H_3$ and I151 $C_\delta H_3$ (*SI Appendix*, Fig. S20*B*), consistent with the FC-binding site being adjacent to L104 and L100 (*SI Appendix*, Fig. S19).

Comparing the ^{15}N/^{1}H HSQC spectra of AIPL1–FKBP WT, V71F, and the N65K/M66K/E70P triple mutant (*SI Appendix*, Figs. S14 and S18), it is clear that the triple mutant gives the best spectrum, and the WT protein gives the worst spectrum, whereas the V71F mutant exhibits an intermediate spectral quality. Different degrees of spectral quality or peak heterogeneity reflect different protein conformational heterogeneity. The β4-α1 loop in the AIPL1–FKBP$^{\Delta 111-132}$:FC complex is known to exhibit heterogeneous conformations in solution (26). Therefore, the β4-α1 loop in apo AIPL1–FKBP is likely very dynamic and contributes to the flip-in and flip-out conformations of the adjacent residue W72. The

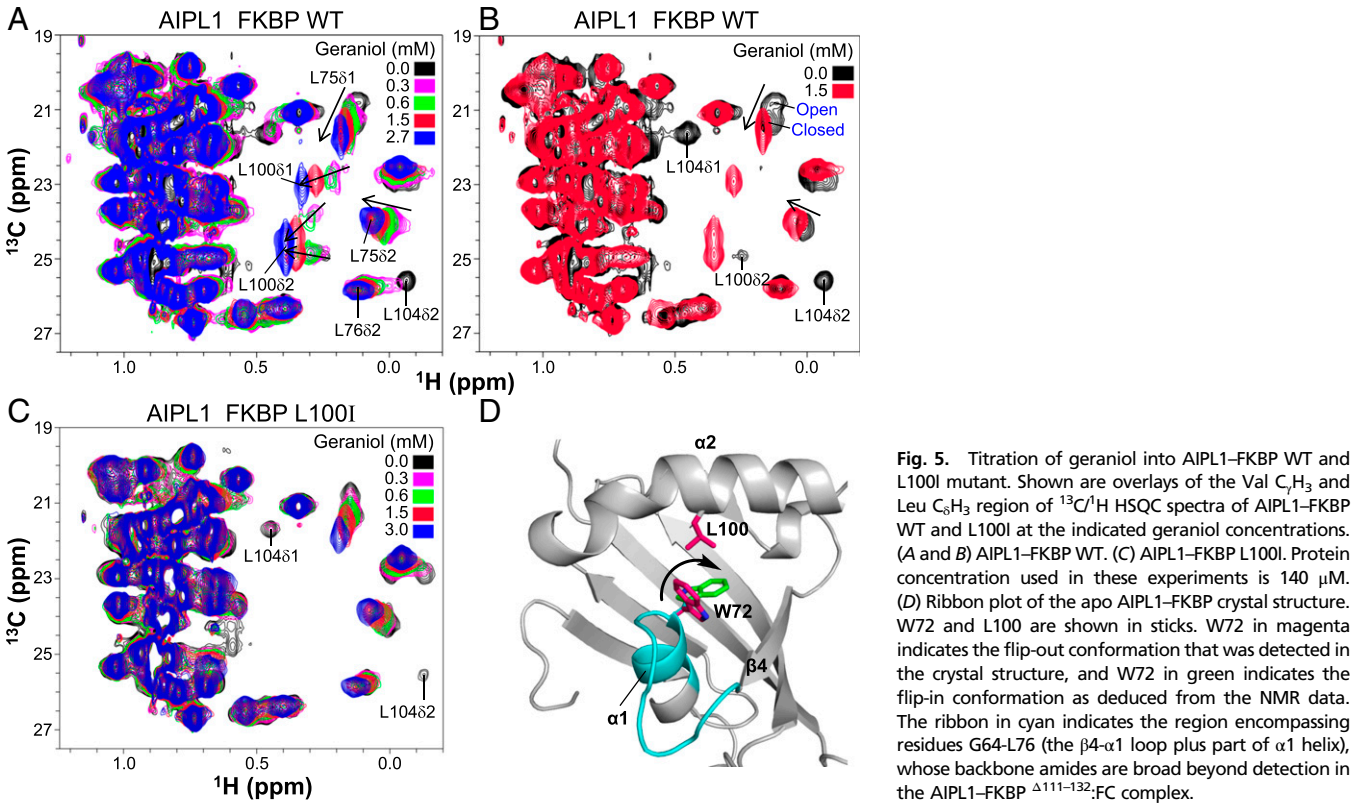

Fig. 5. Titration of geraniol into AIPL1–FKBP WT and L100I mutant. Shown are overlays of the Val $C_\gamma H_3$ and Leu $C_\delta H_3$ region of $^{13}C/^{1}H$ HSQC spectra of AIPL1–FKBP WT and L100I at the indicated geraniol concentrations. (*A* and *B*) AIPL1–FKBP WT. (*C*) AIPL1–FKBP L100I. Protein concentration used in these experiments is 140 μM. (*D*) Ribbon plot of the apo AIPL1–FKBP crystal structure. W72 and L100 are shown in sticks. W72 in magenta indicates the flip-out conformation that was detected in the crystal structure, and W72 in green indicates the flip-in conformation as deduced from the NMR data. The ribbon in cyan indicates the region encompassing residues G64-L76 (the β4-α1 loop plus part of α1 helix), whose backbone amides are broad beyond detection in the AIPL1–FKBP $^{\Delta 111-132}$:FC complex.

triple mutant that mimics β4-α1 loop residues of AIP–FKBP likely has quenched the dynamics of this loop and resulted in a β4-α1 loop-in and W72 flip-in conformation. In contrast, the β4-α1 loop in the V71F mutant likely remains dynamic and heterogeneous, like that in the WT protein, but the increased flip-in conformation of W72 as a result of V71F mutation greatly improved the spectral quality.

MD Simulations. To gain additional insights into probable conformational states of AIPL1–FKBP WT and V71F in solution, we performed MD simulations using the apo structures of AIPL1–FKBP (PDB ID code 5U9A) and its V71F mutant (PDB ID code 5U9K) as the starting models. W72 was generally observed to stay in the flipped-out conformation and moved to block the smaller entrance into the hydrophobic cavity shown in Fig. 2*B* (Fig. 7 *A* and *B*). However, for one of the V71F simulations, F71 pushed against W72, causing it to flip-in into the hydrophobic cavity where it remained for the rest of the 113-ns simulation (Fig. 7*C*). This flipped-in position resembled the position seen for the corresponding W73 in the NMR structure of AIP (Fig. 7*D*). The most flexible portion of both WT and V71F AIPL1–FKBP appears to be α3 (Fig. 7*E*). This helix appears to favor moving toward the entrance of the hydrophobic cavity ("lid closed") shielding the cavity from exposure to the solvent (Fig. 7 *F–H* and *SI Appendix*, Table S1). W116 was often found to move to a position occupied by the prenyl moiety of FC and GGpp in the ligand-bound crystal structures blocking the larger entrance to the hydrophobic cavity in Fig. 2*B*. Only in one simulation of WT AIPL1–FKBP did we find α3 to move away from the cavity entrance ("lid open") toward the position occupied by the disordered α3 region of AIP (Fig. 7*F*).

Discussion

AIPL1 is a photoreceptor-specific chaperone of the visual effector PDE6, and its malfunction leads to blindness (11, 20, 22). Despite this clear indication of the importance of AIPL1, the mechanistic underpinnings of its unique function have remained elusive. The catalytic core of rod PDE6 is a heterodimer of farnesylated PDE6A and geranylgeranylated PDE6B, whereas cone PDE6 is a catalytic homodimer of geranylgeranylated PDE6C subunits (27, 28). Each catalytic PDE6 subunit is associated with one inhibitory Pγ subunit (29). HoloPDE6 is synthesized and assembled in the photoreceptor inner segment, and subsequently traffics to the outer segment, the site of phototransduction (30). Newly synthesized PDE6 molecules undergo isoprenylation of their C-terminal–CAAX box within the cytosol. They subsequently translocate to the cytosolic surface of the endoplasmic reticulum, where the AAX sequence is removed and the Cys residue is carboxymethylated (30, 31). Isoprenylation of PDE6 is essential for its interaction with AIPL1–FKBP and the enzyme folding and assembly by AIPL1 (*SI Appendix*, Fig. S21) (20, 23, 32). This type of interaction is unprecedented among FKBPs, including the closely related AIP (22–24), yet the basis of this unique ability remained uncharacterized before the present study.

The structures of the apo, FC-bound, and GGpp-bound FKBP domain of AIPL1 reported herein reveal remarkable features that enable this protein to form a unique hydrophobic pocket and thus to bind the prenyl modifications of its client. In classic FKBPs, the ligand-binding cavity is bounded by the upper portion of a conical half β-barrel and the central helix that donates a tryptophan side chain to the base of the cavity (5). In most FKBP-domain proteins, including FKBP12, the cavity is exposed to the surface, but in AIP (18) and AIPL1 it is protected by an overhanging insert region that acts as a lid. The β4-α1 loops in FKBP12 and AIP assume loop semi-in and loop-in conformations, respectively, which allow sealing of the cavity in AIP (Figs. 1 and 2). In contrast, the key exclusive attribute of AIPL1–FKBP in the crystal structures is the loop-out conformation of the β4-α1 loop, where it flips away from the cavity and α2, creating a novel path into the hydrophobic pocket. This rearrangement of the pocket involves a hinge-like rotation of W72 out of the base of the cavity compared with FKBP12 and AIP. The flip-out of W72 and a small tilting of α1 make the pocket deeper and help to accommodate isoprenyl ligands. The farnesyl and geranylgeranyl moieties bind to this pocket without causing major structural changes in the backbone of the protein. An important feature of ligand-binding by AIPL1–FKBP is the extensive contribution of α2. Side chains of the

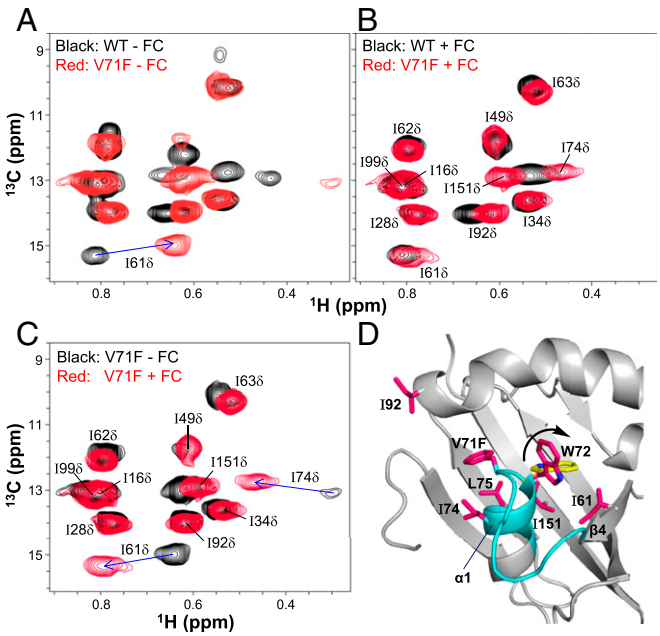

Fig. 6. AIPL1–FKBP V71F has a flip-in major conformation in solution. (*A* and *B*) Overlays of $^{13}C/^{1}H$ HSQC spectra of the Ile $C_{\delta}H_3$ region of AIPL1–FKBP WT and the V71F mutant in the absence and presence of FC, respectively. (*C*) Overlap of the spectra of AIPL1–FKBP V71F in the absence and presence of FC. (*D*) Ribbon plot of the AIPL1–FKBP V71F apo crystal structure, zoomed around V71F. Selected residues are shown in magenta sticks. The NMR data suggest that in the apo protein in solution, the W72 indole ring has rotated into the FC-binding pocket (indicated by yellow stick). The ribbon in cyan indicates the region encompassing residues G64-L76 (the β4-α1 loop plus part of α1 helix), whose backbone amides are broad beyond detection in the AIPL1–FKBP$^{\Delta 111-132}$:FC complex.

α2 residues that make contact with the ligand undergo the most significant repositioning. The contribution of α2 explains an earlier finding that deletion of the insert region abrogates binding of FC to AIPL1 (23). Although the binding of the geranylgeranyl moiety to AIPL1 had been previously hypothesized based on the requirement of AIPL1 for folding of cone PDE6 (24, 32), the structure of AIPL1–FKBP:GG-pp represents direct evidence in support of this interaction. Our data further show that AIPL1–FKBP can bind isoprenoid ligands because it is in the loop-out conformation. Our mutational analysis demonstrates that non-conserved residues in the β4-α1 loop play a key role in inducing this conformation, with the triple mutant form converting it to an AIP-like loop and markedly diminishing its FC-binding ability.

The isoprenyl-binding pocket of AIPL1–FKBP is novel and structurally unrelated to an established lipid-binding fold present in PDD6D, RhoGDI, and Unc119 (33–35). The latter proteins adopt an Ig-like β-sandwich fold that encloses a hydrophobic cavity. PDE6D was originally identified based on copurification with PDE6 from retina extracts (36), and is a ubiquitous prenyl-binding protein that facilitates intracellular trafficking of rod PDE6, rhodopsin kinase, and small GTPases of the Ras-superfamily (37). Thus, structurally different prenyl-binding proteins specialize in folding and trafficking of PDE6.

Remarkably, our NMR analysis of the apo AIPL1–FKBP in solution reveals two major conformations, an open state that is apparently similar to the crystal structure, and a closed (flip-in) state where W72 flips into the ligand-binding pocket. We hypothesize that in the closed state of apo AIPL1–FKBP, the conformation of W72 (and possibly the β4-α1 loop) resembles that in AIP and classic FKBPs. Our data suggest that the apo AIPL1–FKBP in solution exists in equilibrium between the closed and open conformations, and this equilibrium is shifted toward the open and ligand-bound conformations upon binding of FC or GGpp. Paradoxically, as seen from the NMR spectra, the liganded conformation mimics the closed state of the apo AIPL1–FKBP state where W72 occupies the binding pocket and mimics the ligand. Notably, the two conformations of apo AIPL1–FKBP may have provided a clue to the mechanism whereby the W72S and V71F mutations of AIPL1 cause LCA. Although W72 in the flip-in state is predicted to stabilize AIPL1–FKBP, the Ser residue would rather cause destabilization of the protein hydrophobic core, resulting in the observed instability of W72S at physiological temperatures. Although the crystal structures of the apo and FC-bound V71F mutant did not reveal major structural differences relative to the WT protein, our NMR analysis demonstrated that, in solution V71F exists predominantly in the closed conformation, which attenuates ligand binding. This finding is significant because, despite the fact that in our in vitro assays the reduction in FC-FITC binding for the V71F mutant protein was only moderate, in the native environment (where all AIPL1-interacting partners are present) the mutant protein could potentially be locked into the closed conformation, thereby canceling its chaperone activity.

Our MD simulations complemented the finding from NMR in several important aspects. First, they indicated that in the V71F mutant, W72 can indeed transit from the flip-out state to a stable flip-in state. Second, the W72 switch appears not to be strongly coupled to a change of the β4-α1 loop conformation, which remained in the loop-out state. Finally, in the loop-out state, the hydrophobic cavity of apo AIPL1–FKBP can still be shielded from exposure to solvent by the insert α3 containing W116 (G117 in AIP). The shielding of the cavity by α3 in AIPL1–FKBP is apparently dynamic and intermittent to allow isoprenoid binding, whereas the shielding in AIP–FKBP by the loop-in conformation of β4-α1 must be rather stable to block ligand binding.

In conclusion, we solved the crystal structures of apo and isoprenoid-bound AIPL1–FKBP that reveal a structural module for lipid binding that is unique among the FKBP superfamily. Our identification of determinants of the loop-out conformation of AIPL1–FKBP explains why AIPL1 is able to bind isoprenoids. Our NMR analysis uncovered an additional major conformation of the protein involving a conformational switch of the side chain of the key W72 residue. Finally, our data reveal that the LCA-linked V71F mutant protein exists predominantly in the closed conformation, which could account for its pathogenicity. These findings lay the ground for future studies of the structure and mechanisms of the full-length AIPL1 and its interplay with other components of the PDE6 chaperone machinery, such as Pγ and HSP90 (22, 38).

Materials and Methods

Plasmids/Cloning. DNA sequence encoding human AIPL1–FKBP (residues 2–161) was PCR-amplified from a pET15b vector that harbors the AIPL1 cDNA (24), using a 5′ primer with an NcoI site and a His_6 tag, and a 3′ primer with an NdeI site. The PCR product was then cloned into pET15b using the NcoI/NdeI sites. DNA sequences that encode the full-length human AIP and AIP–FKBP (residues 2–169) were PCR-amplified from cDNA isolated from HEK293T cells, and cloned into the pET15b vector using NdeI/XhoI and XbaI/ XhoI sites, respectively. The pET15b and pcDNA3.1 vectors for expression of the full-length mouse AIPL1 was described previously (22, 23).

Chi-AIPL1, in which residues 90–145 of AIPL1 were replaced with residues 91–146 of AIP, was generated in a three-step PCR procedure: (*i*) a DNA sequence encoding AIP_{91-146} was amplified using hybrid AIPL1/AIP primers; (*ii*) this PCR product was used as reverse primer in a PCR with the AIPL1 template; and (*iii*) the new PCR product was then used as a forward primer in a PCR with the AIPL1 template. The chimeric construct was inserted into the NdeI/BamH1 sites of pET15b. A similar PCR protocol was used to generate Chi-AIP, in which residues 91–146 of AIP were replaced with residues 90–145 of AIPL1. Mutations were introduced using the QuikChange protocol for site-directed mutagenesis.

Protein Purification. Chimeric and mutant forms of AIPL1, AIP, AIPL1–FKBP, AIP–FKBP, and AIPL1–AIP were expressed in BL21-(DE3) *Escherichia coli* cells and purified over Ni-NTA resin (EMD Millipore), followed by ion-exchange chromatography on a Mono Q5 column (Bio-Rad), as previously described (23, 24). Final purification was achieved by gel-filtration chromatography on

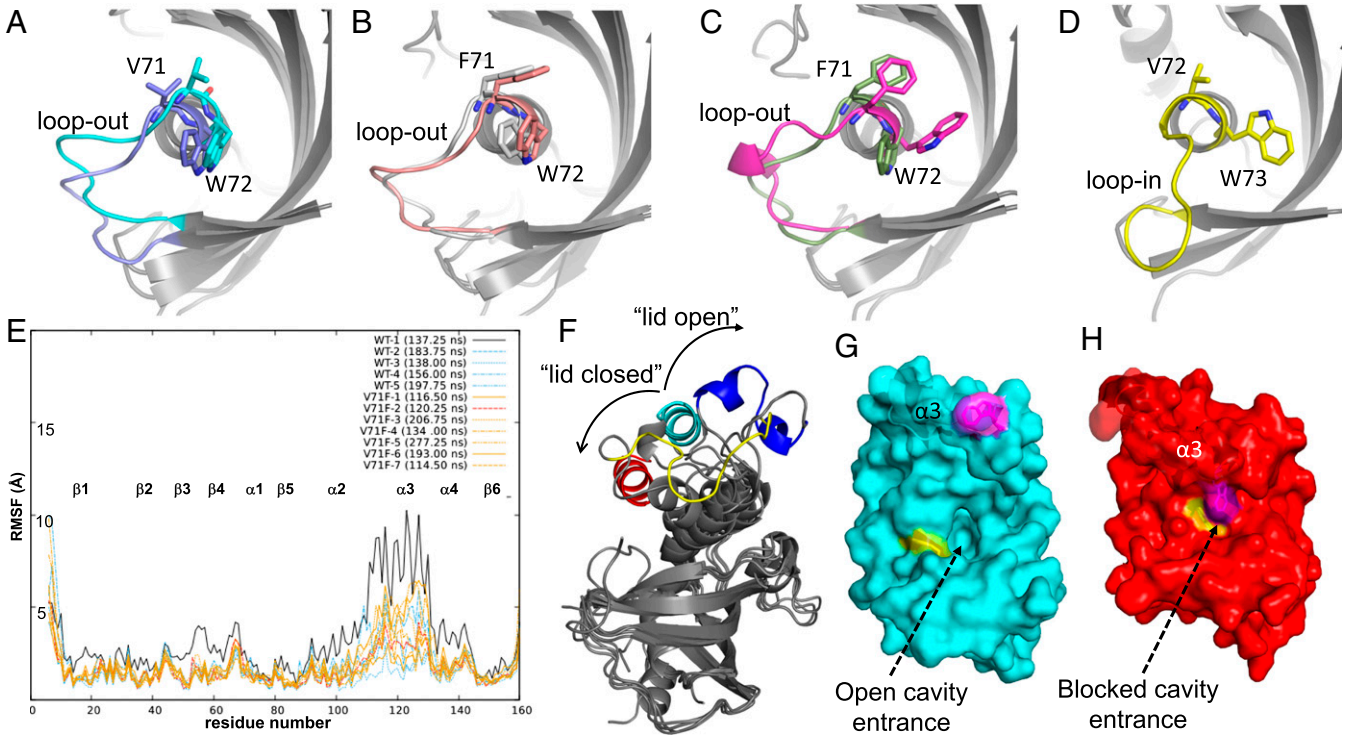

Fig. 7. MD simulations of apo AIPL1–FKBP and V71F. (*A*) Typical WT AIPL1–FKBP run (run 2 in *SI Appendix*, Table S1) (initial model in slate; model at end of 183.75-ns MD simulation in cyan). (*B*) Typical V71F run (run 3; initial model in white; model at end of 206.75 ns in wheat). (*C*) Atypical V71F run (run 2; initial model in green; model at end of 120.25-ns MD simulation in magenta). W72 remains in the flipped-out position in all MD runs of WT AIPL1–FKBP (*A*) and V71F (*B*), except in the MD run V71F-2 (*C*), where movement of F71 caused a clash with W72 and resulted in its immediate flip-in where it remained until the end of the simulation (120 ns). (*D*) The equivalent W73 in AIP was found to be in the flipped-in position. The β4-α1 loop remains in the loop-out position for all WT AIPL1–FKBP and V71F MD runs, suggesting that the flip-in position of W72 may not be strongly coupled to the loop-in β4-α1 loop conformation. (*E*) Root mean square fluctuations for residues in 5 WT FKBP–AIPL1 and 7 V71F independent MD simulations indicating that α3 is the most flexible region. (*F*) Movement of α3 during MD simulations for WT FKBP–AIPL1 from the starting position (cyan) toward the more commonly seen lid-closed (red) position than the lid-open (blue) position seen only in WT-1 simulation (*SI Appendix*, Table S1). AIP's equivalent α3 region is in yellow. (*G*) FKBP–AIPL1 WT structure at the beginning (cyan) and (*H*) after about 180 ns (red) of a MD simulation (WT-2) (*SI Appendix*, Table S1). As the simulation progresses, the entrance to the hydrophobic cavity is blocked by W72 (yellow), which lies near the beginning of α1 and W116 (magenta) which lies near the beginning of α3.

a HiLoad 16/600 Superdex 75 column (GE Healthcare) equilibrated against 50 mM Tris·HCl (pH 7.5) buffer containing 100 mM NaCl and 8 mM DTT.

Uniformly ^{15}N- and ^{13}C-labeled AIPL1-FKBP was obtained according to a protocol outlined previously (26). To obtain uniformly ^{15}N- and selectively ^{13}C-methyl–labeled (for IVL residues) AIPL1–FKBP WT and its mutant forms (39), *E. coli* cells were grown to OD_{600} ~0.6 on enriched 2X-TY medium (2 L), washed three times, and resuspended in 0.5 L M9-minimal medium without any carbon or nitrogen source. After 1-h cell growth at 37 °C, $^{15}NH_4Cl$ (1 g/L), glucose (4 g/L), [$^{13}CH_3$]-labeled α-ketobutyrate (50 mg/L) and [$^{13}CH_3$]-labeled α-ketoisovalerate (100 mg/L) were added, and protein expression was induced by addition of 250 μM isfopropyl-β-D-thiogalactopyranoside (IPTG) and incubated overnight at 18 °C. All isotopes were obtained from Sigma-Aldrich.

Crystallization and Crystal Structure Determination. Purified AIPL1–FKBP and the V71F mutant form of this protein were concentrated to 6–10 mg/mL Stock solutions (30 mM) of the ligands (FC and GGpp) (Enzo Life Sciences) were prepared in DMSO. AIPL1–FKBP and V71F were mixed with FC or GGpp at 1:3 molar ratio and incubated overnight at 4 °C. Crystals of AIPL1–FKBP and V71F, as well as of AIPL1–FKBP:FC, AIPL1–FKBP:GGpp, and V71F:FC were grown by hanging-drop vapor diffusion at 18 °C, against well buffer containing 100 mM Na-citrate, 20% isopropanol and 20% PEG 4000 (pH 5.0–7.0). The crystals grew over periods of 1–3 wk.

Data for the crystals were collected remotely from the University of Iowa Protein Crystallography Facility using the 4.2.2 beamline at the Advanced Light Source (Berkeley, CA). Data were processed using the XDS software (40). Molecular replacement was performed using the MoRDa automatic molecular replacement pipeline (41), which found a crystal structure of FKBP52 (PDB ID code 4LAV) to be the best template for molecular replacement. Although the diffraction data were strongly anisotropic, the structure factors were not explicitly truncated or scaled. Rather, the data were processed conservatively to a slightly lower resolution and scaling for anisotropy was performed during refinement. The refined apo AIPL1–FKBP structure was later used as a template for molecular replacement, performed using the phaser software (42), for the other four structures (AIPL1–FKBP:FC, AIPL1–FKBP:GGpp, V71F, V71F:FC). Structures were refined using REFMAC (43) and phenix.refine (44), and manual models were built using Coot (45). All figures of structures and alignments were generated using the PyMOL Molecular Graphics System (v1.8 Schrödinger, LLC). Diagrams showing interactions of AIPL1–FKBP or V71F with FC and GGpp were generated with LIGPLOT (46). A summary of crystallographic data and refinement statistics for all of the structures is shown in Table 1. Atomic coordinates for the reported structures have been deposited with the Protein Data Bank under accession codes 5U9A (apo AIPL1–FKBP), 5U9I (AIPL1–FKBP:FC), 5U9J (AIPL1–FKBP:GGpp), 5U9K (AIPL1–FKBP V71F), and 5V35 (AIPL1–FKBP V71F:FC).

Fluorescence Binding Assays. FC (3 mM) was labeled with FITC (6 mM) in 100 mM $NaHCO_3$ (pH 8.0) for 1 h at 25 °C, and the FC-FITC product was purified by reverse-phase HPLC. A fluorescence polarization assay was used to measure the binding of FC-FITC (20 nM) to the AIPL1 and AIP proteins, using a HORIBA Jobin Yvon Fluorescence Spectrophotometer with excitation at 490 nm and emission at 520 nm. Labeling of FC with AMCA and a FRET assay of assessing the binding of FC-AMCA to AIPL1–FKBP and V71F were performed using an F-2700 Fluorescence Spectrophotometer (Hitachi), as described previously (23, 24).

NMR Spectroscopy. All NMR spectra were acquired on a 800 MHz Bruker Avance II NMR spectrometer at 25 °C, using uniformly ^{15}N- and selectively ^{13}C-methyl–labeled (for IVL residues) AIPL1–FKBP proteins (WT and mutant

forms) at protein concentration of ~150 μM either in the apo form or in complex with FC in a buffer containing 25 mM sodium phosphate (pH 7.5) and 8 mM DTT in 90% H_2O/10% D_2O. The AIPL1–FKBP/FC complex was prepared by incubating 500 μl of 150 μM protein with 2.2 μL of 230 mM concentrated FC stock that was dissolved in deuterated DMSO overnight on a shaker. The amount of DMSO present in the sample was generally <2%. The excess amount of FC was removed by centrifugation before the NMR experiments were conducted. The samples were analyzed by acquiring $^{15}N/^{1}H$ and $^{13}C/^{1}H$ HSQC spectra. The ^{1}H chemical shifts are referenced to 2,2-dimethyl-2-silapentane-5-sulfonate. The collected data were processed using NMRPipe (47) and analyzed using NMRView (48).

MD Simulations. MD simulations were performed with YASARA Structure 16.7.22 using the md_runfast macro. The AIPL1–FKBP domain WT (PDB ID code 5U9A) and V71F (PDB ID code 5U9K) apo structures determined at 2.7 Å in the $C222_1$ space group were used as starting models for the MD. The simulations were run using the AMBER14 force field in water at a temperature of 298 K, pH of 7.4 and NaCl concentration of 0.9%. Particle mesh Ewald summation was used to compute long-range columbic interactions with a periodic cell boundary and a cutoff of 8 A. Five independent MD runs were performed for WT and seven for V71F with simulation times ranging from about 114–277 ns (*SI Appendix*, Table S1).

Dynamic Light Scattering. DLS was used to examine the degree of polydispersity and thermostability of AIPL1–FKBP and mutant samples. Purified AIPL1–FKBP and mutants were concentrated up to 3 mg/mL and used for light-scattering experiments. The FC-bound AIPL1–FKBP samples were prepared as described for crystallization and filtered through 0.02-μm syringe filters (Sigma-Aldrich). DLS data for thermostability measurements were collected while heating the samples from 20 °C to 80 °C at 1 °C/min. Onset of protein thermal unfolding (T_{onset}) was determined by the sudden increase in hydrodynamic radius during the temperature ramp. Analyses of thermostability of AIPL1–FKBP and mutant samples were performed using a DynaPro Nanostar instrument (Wyatt) and data were analyzed using the Dynamics 7.1.7 software.

ACKNOWLEDGMENTS. We thank Jay Nix (Molecular Biology Consortium 4.2.2 beamline at Advanced Light Source) for aid in remote data collection. This research used resources of the Advanced Light Source, which is a Department of Energy Office of Science user facility under Contract DE-AC02-05CH11231. This work was supported by the National Institutes of Health Grant EY-10843 (to N.O.A.).

1. Tong M, Jiang Y (2015) FK506-binding proteins and their diverse functions. *Curr Mol Pharmacol* 9:48–65.
2. Hausch F (2015) FKBPs and their role in neuronal signaling. *Biochim Biophys Acta* 1850:2035–2040.
3. Storer CL, Dickey CA, Galigniana MD, Rein T, Cox MB (2011) FKBP51 and FKBP52 in signaling and disease. *Trends Endocrinol Metab* 22:481–490.
4. MacMillan D (2013) FK506 binding proteins: Cellular regulators of intracellular Ca2+ signalling. *Eur J Pharmacol* 700:181–193.
5. Van Duyne GD, Standaert RF, Karplus PA, Schreiber SL, Clardy J (1993) Atomic structures of the human immunophilin FKBP-12 complexes with FK506 and rapamycin. *J Mol Biol* 229:105–124.
6. Blackburn EA, Walkinshaw MD (2011) Targeting FKBP isoforms with small-molecule ligands. *Curr Opin Pharmacol* 11:365–371.
7. Sigal NH, Dumont FJ (1992) Cyclosporin A, FK-506, and rapamycin: Pharmacologic probes of lymphocyte signal transduction. *Annu Rev Immunol* 10:519–560.
8. Fanghanel J, Fischer G (2004) Insights into the catalytic mechanism of peptidyl prolyl *cis/trans* isomerases. *Front Biosci* 9:3453–3478.
9. Alag R, et al. (2013) Structural insights into substrate binding by PvFKBP35, a peptidylprolyl *cis-trans* isomerase from the human malarial parasite *Plasmodium vivax*. *Eukaryot Cell* 12:627–634.
10. Huse M, Chen YG, Massagué J, Kuriyan J (1999) Crystal structure of the cytoplasmic domain of the type I TGF beta receptor in complex with FKBP12. *Cell* 96:425–436.
11. Sohocki MM, et al. (2000) Mutations in a new photoreceptor-pineal gene on 17p cause Leber congenital amaurosis. *Nat Genet* 24:79–83.
12. Koenekoop RK (2004) An overview of Leber congenital amaurosis: A model to understand human retinal development. *Surv Ophthalmol* 49:379–398.
13. Sohocki MM, et al. (2000) Prevalence of AIPL1 mutations in inherited retinal degenerative disease. *Mol Genet Metab* 70:142–150.
14. Dharmaraj S, et al. (2004) The phenotype of Leber congenital amaurosis in patients with AIPL1 mutations. *Arch Ophthalmol* 122:1029–1037.
15. Stone EM (2007) Leber congenital amaurosis—A model for efficient genetic testing of heterogeneous disorders: LXIV Edward Jackson Memorial Lecture. *Am J Ophthalmol* 144:791–811.
16. van der Spuy J, et al. (2002) The Leber congenital amaurosis gene product AIPL1 is localized exclusively in rod photoreceptors of the adult human retina. *Hum Mol Genet* 11:823–831.
17. Trivellin G, Korbonits M (2011) AIP and its interacting partners. *J Endocrinol* 210: 137–155.
18. Linnert M, et al. (2013) The FKBP-type domain of the human aryl hydrocarbon receptor-interacting protein reveals an unusual Hsp90 interaction. *Biochemistry* 52:2097–2107.
19. Li J, et al. (2013) Unique proline-rich domain regulates the chaperone function of AIPL1. *Biochemistry* 52:2089–2096.
20. Ramamurthy V, Niemi GA, Reh TA, Hurley JB (2004) Leber congenital amaurosis linked to AIPL1: A mouse model reveals destabilization of cGMP phosphodiesterase. *Proc Natl Acad Sci USA* 101:13897–13902.
21. Liu X, et al. (2004) AIPL1, the protein that is defective in Leber congenital amaurosis, is essential for the biosynthesis of retinal rod cGMP phosphodiesterase. *Proc Natl Acad Sci USA* 101:13903–13908.
22. Gopalakrishna KN, Boyd K, Yadav RP, Artemyev NO (2016) Aryl hydrocarbon receptor-interacting protein-like 1 is an obligate chaperone of phosphodiesterase 6 and is assisted by the γ-subunit of its client. *J Biol Chem* 291:16282–16291.
23. Majumder A, Gopalakrishna KN, Cheguru P, Gakhar L, Artemyev NO (2013) Interaction of aryl hydrocarbon receptor-interacting protein-like 1 with the farnesyl moiety. *J Biol Chem* 288:21320–21328.
24. Yadav RP, Majumder A, Gakhar L, Artemyev NO (2015) Extended conformation of the proline-rich domain of human aryl hydrocarbon receptor-interacting protein-like 1: Implications for retina disease. *J Neurochem* 135:165–175.
25. Kleywegt GJ, Jones TA (1994) Detection, delineation, measurement and display of cavities in macromolecular structures. *Acta Crystallogr D Biol Crystallogr* 50:178–185.
26. Yu L, Yadav RP, Artemyev NO (2017) NMR resonance assignments of the FKBP domain of human aryl hydrocarbon receptor-interacting protein-like 1 (AIPL1) in complex with a farnesyl ligand. *Biomol NMR Assign* 11:111–115.
27. Anant JS, et al. (1992) In vivo differential prenylation of retinal cyclic GMP phosphodiesterase catalytic subunits. *J Biol Chem* 267:687–690.
28. Qin N, Baehr W (1994) Expression and mutagenesis of mouse rod photoreceptor cGMP phosphodiesterase. *J Biol Chem* 269:3265–3271.
29. Deterre P, Bigay J, Forquet F, Robert M, Chabre M (1988) cGMP phosphodiesterase of retinal rods is regulated by two inhibitory subunits. *Proc Natl Acad Sci USA* 85: 2424–2428.
30. Karan S, Zhang H, Li S, Frederick JM, Baehr W (2008) A model for transport of membrane-associated phototransduction polypeptides in rod and cone photoreceptor inner segments. *Vision Res* 48:442–452.
31. Wang M, Casey PJ (2016) Protein prenylation: Unique fats make their mark on biology. *Nat Rev Mol Cell Biol* 17:110–122.
32. Kolandaivelu S, Ramamurthy V (2014) AIPL1 protein and its indispensable role in cone photoreceptor function and survival. *Adv Exp Med Biol* 801:43–48.
33. Hanzal-Bayer M, Renault L, Roversi P, Wittinghofer A, Hillig RC (2002) The complex of Arl2-GTP and PDE delta: From structure to function. *EMBO J* 21:2095–2106.
34. Hoffman GR, Nassar N, Cerione RA (2000) Structure of the Rho family GTP-binding protein Cdc42 in complex with the multifunctional regulator RhoGDI. *Cell* 100:345–356.
35. Zhang H, et al. (2011) UNC119 is required for G protein trafficking in sensory neurons. *Nat Neurosci* 14:874–880.
36. Gillespie PG, Prusti RK, Apel ED, Beavo JA (1989) A soluble form of bovine rod photoreceptor phosphodiesterase has a novel 15-kDa subunit. *J Biol Chem* 264:12187–12193.
37. Baehr W (2014) Membrane protein transport in photoreceptors: The function of PDEδ: the Proctor lecture. *Invest Ophthalmol Vis Sci* 55:8653–8666.
38. Hidalgo-de-Quintana J, Evans RJ, Cheetham ME, van der Spuy J (2008) The Leber congenital amaurosis protein AIPL1 functions as part of a chaperone heterocomplex. *Invest Ophthalmol Vis Sci* 49:2878–2887.
39. Marley J, Lu M, Bracken C (2001) A method for efficient isotopic labeling of recombinant proteins. *J Biomol NMR* 20:71–75.
40. Kabsch W (2010) XDS. *Acta Crystallogr D Biol Crystallogr* 66:125–132.
41. Vagin A, Lebedev A (2015) MoRDa, an automatic molecular replacement pipeline. *Acta Crystallogr A* 71:S19.
42. Read RJ (2001) Pushing the boundaries of molecular replacement with maximum likelihood. *Acta Crystallogr D Biol Crystallogr* 57:1373–1382.
43. Murshudov GN, et al. (2011) REFMAC5 for the refinement of macromolecular crystal structures. *Acta Crystallogr D Biol Crystallogr* 67:355–367.
44. Adams PD, et al. (2010) PHENIX: A comprehensive Python-based system for macromolecular structure solution. *Acta Crystallogr D Biol Crystallogr* 66:213–221.
45. Emsley P, Cowtan K (2004) Coot: Model-building tools for molecular graphics. *Acta Crystallogr D Biol Crystallogr* 60:2126–2132.
46. Wallace AC, Laskowski RA, Thornton JM (1995) LIGPLOT: A program to generate schematic diagrams of protein-ligand interactions. *Protein Eng* 8:127–134.
47. Delaglio F, et al. (1995) NMRPipe: A multidimensional spectral processing system based on UNIX pipes. *J Biomol NMR* 6:277–293.
48. Johnson BA, Blevins RA (1994) NMR View: A computer program for the visualization and analysis of NMR data. *J Biomol NMR* 4:603–614.